RSCPublishing   Faraday Discussions

Identifying pragmatic quasi-harmonic electronic structure approaches for modeling molecular crystal thermal expansion

SCHOLARONE™
Manuscripts

Journal Name

Identifying pragmatic quasi-harmonic electronic structure approaches for modeling molecular crystal thermal expansion[†]

Jessica L. McKinley[a] and Gregory J. O. Beran[*a]

Quasi-harmonic approaches provide an economical route to modeling the temperature dependence of molecular crystal structures and properties. Several studies have demonstrated good performance of these models, at least for rigid molecules, when using fragment-based approaches with correlated wavefunction techniques. Many others have found success employing dispersion-corrected density functional theory (DFT). Here, a hierarchy of models in which the energies, geometries, and phonons are computed either with correlated methods or DFT are examined to identify which combinations produce useful predictions for properties such as the molar volume, enthalpy, and entropy as a function of temperature. The results demonstrate that refining DFT geometries and phonons with single-point energies based on dispersion-corrected second-order Møller-Plesset perturbation theory can provide clear improvements in the molar volumes and enthalpies compared to those obtained from DFT alone. Predicted entropies, which are governed by vibrational contributions, benefit less clearly from the hybrid schemes. Using these hybrid techniques, the room-temperature thermochemistry of acetaminophen (paracetamol) is predicted to address the discrepancy between two experimental sublimation enthalpy measurements.

1 Introduction

Molecular crystals occur in many areas of chemistry, including pharmaceuticals, organic semi-conductor materials, foods, and explosives. Crystal structure and polymorphism, or the tendency for molecules to adopt multiple distinct crystalline packing motifs, can have substantial impacts on macroscopic properties of these materials. The difficulty in identifying or engineering crystal forms experimentally has generated considerable interest in predicting crystal structures and properties from first principles.[1–3] Substantial progress has been made toward successful crystal structure prediction, as evidenced by the successes in the last few Blind Tests of Crystal Structure Prediction.[4–6]

Most molecular crystal modeling focuses on the 0 K electronic (internal) energy rather than the finite-temperature free energy.[7] However, temperature can play an important role in many molecular crystal properties. Crystals typically undergo thermal expansion, often at a rate of 0.8–2.5% expansion per 100 K.[8] Even larger expansion occurs in weakly bound crystals. As the crys-

tal expands, its mechanical properties change. Bulk moduli often decrease by 50% and shear moduli by 30–50% at temperatures approaching the melting point.[8]

The Gibbs free energy also varies with temperature, with room-temperature values typically differing by 1–4 kJ/mol from the 0 K electronic energy.[8,9] Thermal expansion typically softens the lattice vibrations, resulting in a larger Helmholtz vibrational entropy, while simultaneously decreasing the lattice energy. Early investigations suggested that entropic effects were seldom large enough to reverse polymorph stability.[10] Though a significant fraction of the finite-temperature contribution cancels when considering polymorph energy differences, a more recent survey noted that at least 20% of polymorphs pairs are enantiotropically related and reverse their relative thermodynamic stabilities upon heating.[8] Many other properties, including vibrational[11] and nuclear magnetic resonance spectroscopic properties vary with the unit cell size, as well.

Various strategies exist for incorporating finite temperature contributions into the model. Molecular dynamics techniques provide a natural means of treating these effects.[12–21] However, obtaining force fields capable of describing the subtle energetic balances that occur in molecular crystal problems is not always easy. Alternatively, one can employ statistical thermodynamic harmonic or quasi-harmonic corrections to static models.[11] Har-

[a] Department of Chemistry, University of California, Riverside, California 92521 USA; E-mail: gregory.beran@ucr.edu

monic phonon contributions are increasingly being employed in crystal structure prediction,[6] and they capture a significant fraction of the vibrational contribution to the free energy.[8,22] Harmonic vibrational contributions impact the polymorph stability ordering in glycine,[23,24], oxalyl dihydrazide,[25] aspirin,[26] and modern drug targets,[27] for example.

However, to capture thermal expansion effects, one must address how the phonons change with crystal volume. The quasi-harmonic approximation provides a straightforward means for doing so and for therefore predicting how the Gibbs free energy depends on temperature and pressure. The quasi-harmonic approximation has been used long been used in force field studies.[28–33] Recent DFT work has examined how free energy impacts structure rankings in crystal structure prediction.[34,35] It has sought to reproduce structural and thermochemical properties of crystalline ammonia,[11] urea,[36] and carbamazepine (using density functional tight binding theory).[37]

These DFT-based quasi-harmonic studies have been successful, and wavefunction-based techniques are often too computationally demanding for quasi-harmonic crystal studies. However, fragment approaches such as the hybrid many-body interaction (HMBI) model, enable application of high-level, correlated wavefunction techniques that would otherwise be computationally prohibitive to molecular crystal problems. HMBI combines a quantum mechanical (QM) treatment of the unit cell monomers and their short-range dimer interactions with a classical polarizable force field treatment of longer-range and many-body effects.[38–41] We have demonstrated that the quasi-harmonic HMBI[42] with large-basis second-order Møller-Plesset perturbation theory (MP2) and/or coupled clusters singles and doubles with perturbative triples (CCSD(T)) allows prediction of small-molecule structures and properties in excellent agreement with experiment. For example, it predicts the thermal expansion of carbon dioxide phase I to within 2–3%, the sublimation enthalpy to within 1–2 kJ/mol, and the sublimation temperature to within 3 K.[9,43] By comparing and contrasting the excellent agreement between theory and experimental structures and Raman spectra for several different crystalline phases of carbon dioxide, we argued that the long-accepted structure for phase III carbon dioxide is incorrect, and that phases III and VII are actually identical.[44] Furthermore, these same techniques enabled successful prediction of crystalline methanol thermochemistry.[45] More significantly, they allow *ab initio* prediction of the polymorph phase diagram with accuracy corresponding to Gibbs free energy errors of ∼0.5 kJ/mol or less.[46] Other fragment-based studies have similarly employed the quasi-harmonic approximation to study thermochemical properties in a much broader range of crystals.[47,48]

However, even with fragment techniques, the studies employing correlated wavefunction methods are computationally demanding. Predicting the methanol phase diagram entirely with MP2 and CCSD(T) required several hundred thousand central processing unit hours, for example. Performing the same level calculations on a typical pharmaceutical crystal would be impractical. Is there a useful middle ground, which achieves most of the accuracy found above, albeit at much lower computational cost?

A quasi-harmonic calculation involves three main ingredients:

energies, crystal geometries, and phonon frequencies. This study investigates how accurately one must compute each of those pieces to predict how crystal structures vary with temperature accurately. Can one, for example, replace a computationally expensive MP2 treatment of the phonon frequencies with a less-demanding one from periodic DFT? What about the geometries? Or, taken from the opposite perspective in which dispersion-corrected DFT models are the baseline: How much do the predicted finite-temperature structures or thermochemistry benefit by investing the additional computational effort to replace some or all of these quasi-harmonic approximation components with results obtained from correlated wave function methods? Even inexpensive semi-empirical density functional tight binding models reproduce the thermal expansion in carbamazepine fairly well,[37] for example.

Here, to improve our understanding of how the performance of correlated wavefunction and DFT methods compare and the potential benefits of combining them in different ways, we examine the thermal expansion in several small-molecule crystals, systematically replacing the MP2 (or better) treatment of the energies, structures, and/or phonons with a dispersion-corrected DFT one. We find that while portions of the calculation can often be performed with periodic density functional theory, there are clear benefits to including contributions from wavefunction techniques. Based on the results from the small molecule systems, quasi-harmonic calculations are performed on the pharmaceutical acetaminophen (paracetamol) to predict both the thermal expansion and to investigate a discrepancy between two experimentally reported heats of sublimation.

2 Theory

2.1 Quasi-Harmonic Approximation

The Gibbs free energy is required to model molecular crystals at finite temperatures and pressures. From statistical thermodynamics, the Gibbs free energy combines the electronic internal energy U_{el}, the Helmholtz vibrational free energy F_{vib}, and a pressure-volume (PV) contribution,

$$G(T,P) = U_{el} + F_{vib}(T) + PV \qquad (1)$$

In crystals at ambient pressure, the PV term contributes negligibly.

The internal electronic energy U_{el} is computed here via the fragment-based hybrid many-body interaction model (HMBI). HMBI treats individual molecules in the unit cell and their short-range pairwise interactions quantum mechanically (QM), while the longer-range and many-body interactions are typically approximated using a classical molecular mechanics (MM) polarizable force field.

$$U_{el}^{HMBI} = E_{1-body}^{QM} + E_{SR\ 2-body}^{QM} + E_{LR\ 2-body}^{MM} + E_{many\ body}^{MM} \qquad (2)$$

In some cases, the MM terms will be computed from periodic Hartree-Fock (HF) instead, in which case HMBI is equivalent to the method of increments.[49–51]

The Helmholtz vibrational free energy is computed from stan-

Table 1 The four model tiers considered in this work. Tier 1 is the most computationally demanding, and higher tiers subsequently reduce the computational cost by replacing portions of calculations at the "High" HMBI level with faster ones at the "Low" level of theory, DFT. HMBI corresponds to employing MP2 or other correlated wavefunction methods for the monomer and dimer treatment plus AMOEBA or periodic HF many-body contributions.

Tier	Energies	Structures	Frequencies
1	HMBI	HMBI	HMBI
2	HMBI	HMBI	DFT
3	HMBI	DFT	DFT
4	DFT	DFT	DFT

dard harmonic oscillator vibrational partition functions as,

$$F_{vib}(T) = N_a \sum_i \left(\frac{\hbar \omega_i}{2} + k_b T \ln \left[1 - \exp\left(-\frac{\hbar \omega_i}{k_b T} \right) \right] \right) \quad (3)$$

where N_a is Avogadro's number, $\hbar$ is Plank's constant, k_b is the Boltzmann constant, and ω_i is the vibrational frequency of mode i. The first term corresponds to the zero-point vibrational contribution, while the second gives the thermal vibrational contribution. Here, phonons are evaluated only at the Γ point.

To circumvent the high computational cost of computing the phonons repeatedly while minimizing $G(T,P)$ for the given thermodynamic conditions, the vibrational contribution can be approximated via the quasi-harmonic approximation, which estimates how the phonon frequencies and F_{vib} vary with unit cell volume. Mode-specific Grüneisen parameters γ_i are employed to estimate how each individual phonon frequency varies with volume,

$$\gamma_i = -\left(\frac{\partial \ln \omega_i}{\partial \ln V} \right) \quad (4)$$

Integrating this equation yields,

$$\omega_i = \omega_i^{ref} \left(\frac{V}{V^{ref}} \right)^{-\gamma_i} \quad (5)$$

The reference volumes and phonon frequencies are obtained for the crystal structures which minimize the electronic energy U_{el}, and the Grüneisen parameters are obtained via finite difference of the phonon frequencies with respect to changes in unit cell volume about that reference structure.

2.2 Hierarchy of Approximations

The key question addressed in this study is how accurately one needs to compute each ingredient in the quasi-harmonic model: the energies, crystal geometries, and the phonon frequencies. Previous work has demonstrated that evaluating all three ingredients with HMBI using large-basis MP2 often performs very well (subject to the well-known limitations of MP2[51]), and even better results are obtained if the single-point energies are refined with a CCSD(T) treatment of the HMBI monomers and dimers. However, large-basis correlated wave function method calculations can be computationally expensive. Here, a systematic hierarchy of four different tiers of approximation is adopted, as summarized in Table 1.

In Tier 1, all calculations are performed at the "High" level of theory—optimizing the structures, computing the phonons, and in some cases refining the single-point energies with correlated wavefunction methods via HMBI. Single-point energy refinement might include using larger basis sets, employing CCSD(T) or MP2C instead of MP2, or calculating the many-body contributions from periodic HF instead of AMOEBA. AMOEBA models electrostatics with atom-centered multipole moments up to quadrupoles, polarization with self-consistently induced dipoles and a Thole damping model, and van der Waals via a buffered 14-7 potential.[52] Although Tier 1 performs well,[9,43–46] it is computationally demanding and quickly becomes impractical beyond several dozen atoms per unit cell (assuming $P2_1/c$ symmetry or similar).

Tier 2 replaces the single most computationally demanding portion of the calculation, the HMBI phonon frequency evaluation, with phonons at the "Low" level, periodic DFT. Because harmonic frequency calculations require that the system geometry be at a stationary point of the potential energy surface with respect to the atomic positions, Tier 2 structures optimized with HMBI then have their atomic positions relaxed with DFT while the lattice parameters being held fixed at their HMBI values. This ensures real vibrational frequencies while maintaining the (hopefully) more reliable HMBI unit cell. Because the unit cell is constrained, the DFT relaxation typically alters the atomic positions only slightly.

A similar approach was previously used to predict pressure-dependent Raman spectra for several phases of carbon dioxide in excellent agreement with experiment.[44] In that instance, the unit cell was first predicted at the quasi-harmonic HMBI MP2/CBS limit, and then atomic positions were relaxed and Raman spectrum predicted at the HMBI MP2/aug-cc-pVDZ level to reduce the computational cost of the phonon evaluation. Constraining the cell at the dimensions predicted with the large basis set helped ensure the key lattice phonon modes were reproduced correctly despite the small basis set.

Tier 3 seeks to reduce the computational costs further, performing all structure optimizations and phonon frequency evaluations with periodic DFT. Only single-point energies are computed from wave function methods with HMBI. Depending on the electronic structure method used for the monomers and dimers in the HMBI single-point energies, the computational cost of Tier 3 can be only moderately higher than a pure DFT calculation (Tier 4).

Our recent studies of crystalline methanol,[45,46] which considered a complete basis set (CBS) CCSD(T) HMBI treatment on geometries from either MP2/CBS HMBI (Tier 1) or periodic PBE-D3 calculations (Tier 3). In the initial work,[45] it was unclear how much better Tier 1 was than Tier 3. For example, the sublimation enthalpy was more accurate when computed from MP2 structures, while thermal expansion agreed more closely with experiment when using the DFT structures. Subsequently, we recognized that AMOEBA was overestimating the many-body contribution. Replacing that AMOEBA contribution with one computed from periodic HF in the final single-point energies significantly improved the quality of the predictions using the MP2 geometries, while those using the PBE-D3 geometries became slightly worse.[46] In the present work, examining several additional crys-
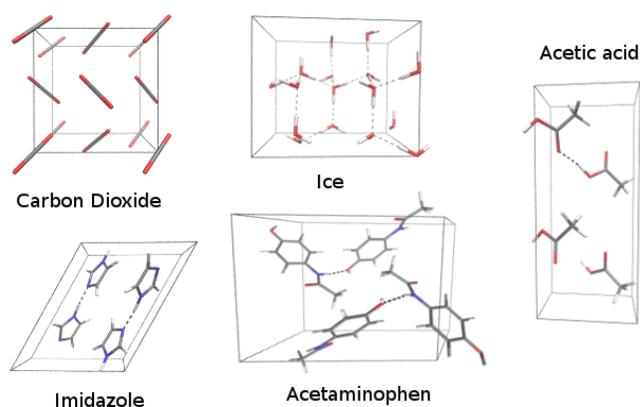
Fig. 1 The crystals modeled in this study.

tals will provide further insights into the performance of Tier 3 models.

Finally, Tier 4 performs all calculations with periodic DFT. Many quasi-harmonic studies in the literature already employ this approach. Here, Tier 4 provides a baseline for assessing what, if any, improvement one finds upon incorporating energies, structures, or phonons from correlated wavefunction techniques on top of DFT. Of course, many different density functionals and dispersion corrections exist, and the results will depend somewhat on the particular model choices.

2.3 Computational details

To evaluate the performance of the different hybrid tiers described in Section 2.2, we return to the four small-molecule crystals whose thermal expansion was previously investigated with Tier 1:[9,43] carbon dioxide phase I, ice Ih, acetic acid (orthorhombic phase), and α imidazole (Figure 1). Initial crystal structures were taken from a low-temperature experimental crystal structure of carbon dioxide,[53] a zero net dipole 16-molecule supercell of ice,[54] a 278 K single crystal x-ray diffraction structure of acetic acid (Cambridge Crystal Structure Database (CSD) reference code ACETAC01),[55] and a 103 K neutron scattering structure of imidazole (IMAZOL06).[56] To investigate the performance on larger species, results are also presented for acetaminophen form I (monoclinic form) starting from a 20 K neutron scattering structure (HXACAN13)[57]. Experimental temperature-dependent volume data was found in the literature for carbon dioxide,[58] ice,[59] acetic acid,[55,60], and imidazole.[56,61,62] Enthalpy and entropy data for carbon dioxide,[63–66] ice,[67–69] acetic acid,[68,70,71] and imidazole[72–74] were taken or derived from experimental data, as described previously.[9]

All Tier 1 results here were taken from our earlier work in Ref 9. Those were obtained by minimizing the Gibbs free energy (Eq 1) on the fly at each temperature with quasi-harmonic evaluation of the phonon contribution. In that work, the Grüneisen parameters were computed by isotropically expanding and contracting the lattice by 10 Å^3 in order to approximate the derivative in Eq 4 via finite difference. Ice and carbon dioxide do in fact expand nearly isotropically. The other two crystals exhibit slightly

more anisotropic expansion, so one might prefer an approach that estimates the Grüneisen parameters based on anisotropic volume changes. Nevertheless, agreement between the predicted and experimental volumes are fairly reasonable. Note that the PV term contributes negligibly at ambient pressure and was neglected in all cases. Also, slight irregularities occur in some of the Tier 1 thermal expansion results due to numerical convergence issues on the generally flat energy surfaces.

For the new Tier 2–4 results here, a slightly different approach is taken. First, energy versus volume curves $E(V)$ were mapped out as a function of volume, by minimizing the HMBI or DFT energy of the cell under positive (cell compression) or negative pressure (cell expansion). The resulting $E(V)$ curve was fitted to the Murnaghan equation of state,

$$E(V) = E_0 + \frac{B_0 V}{B_0'} \left[\frac{(V_0/V)^{B_0'}}{B_0' - 1} + 1 \right] - \frac{B_0 V_0}{B_0' - 1} \qquad (6)$$

where E_0, V_0, B_0, and B_0' are the fit parameters. E_0 gives the electronic energy at the minimum, V_0 is the molar volume at the minimum energy, B_0 is the bulk modulus, and B_0' is the first derivative of the bulk modulus with respect to pressure.

Next, the reference phonon frequencies and Grüneisen parameters were computed. Instead of isotropically scaling the crystal volumes in the finite difference estimate of Eq 4, frequencies were computed on the positive and negative pressure structures surrounding the electronic energy minimum. This anisotropic estimate for the Grüneisen parameters should provide a better description for how the phonons vary with volume. Using Eqs 3 and 5, the Helmholtz vibrational free energy F_{vib} was calculated as a function of volume for various temperatures and cubically splined. Care was taken to ensure that explicit data points extend outside the actual volume range to avoid spline artifacts in the region of interest. Summing the fitted $E(V)$ and splined F_{vib} contributions (neglecting the PV term at ambient pressure) gives the Gibbs free energy as a function of volume and temperature. Minimizing $G(V,T)$ with respect to volume provides the optimal unit cell structure at that temperature. Selected crystalline energy-volume curves, Helmholtz vibrational free energies, and Gibbs free energies are provided in ESI Figures S1–S4.

Enthalpy and entropy were computed from the same ingredients using the standard statistical mechanical expression. See Ref 43 for details. Similarly, standard ideal gas, rigid rotor, and harmonic oscillator partition function expressions were used to evaluate thermochemical contributions for the gas phase species when computing sublimation enthalpies and entropies.

For HMBI, density-fitted MP2 were carried out in the Dunning aug-cc-pVXZ basis sets (X = D, T, or Q, and abbreviated aXZ in some places) using Molpro v2012.1[75] Because MP2 has well-known problems with van der Waals dispersion, we also refined some single-point energies with MP2C,[76,77] also using Molpro. MP2C replaces the uncoupled HF treatment of dispersion found in MP2 with an improved coupled Kohn-Sham treatment, and it performs very well for non-covalent interactions.[78] Because the MP2C dispersion correction is less sensitive to basis set than MP2,[79] the correction was computed in the aug-cc-pVTZ basis set
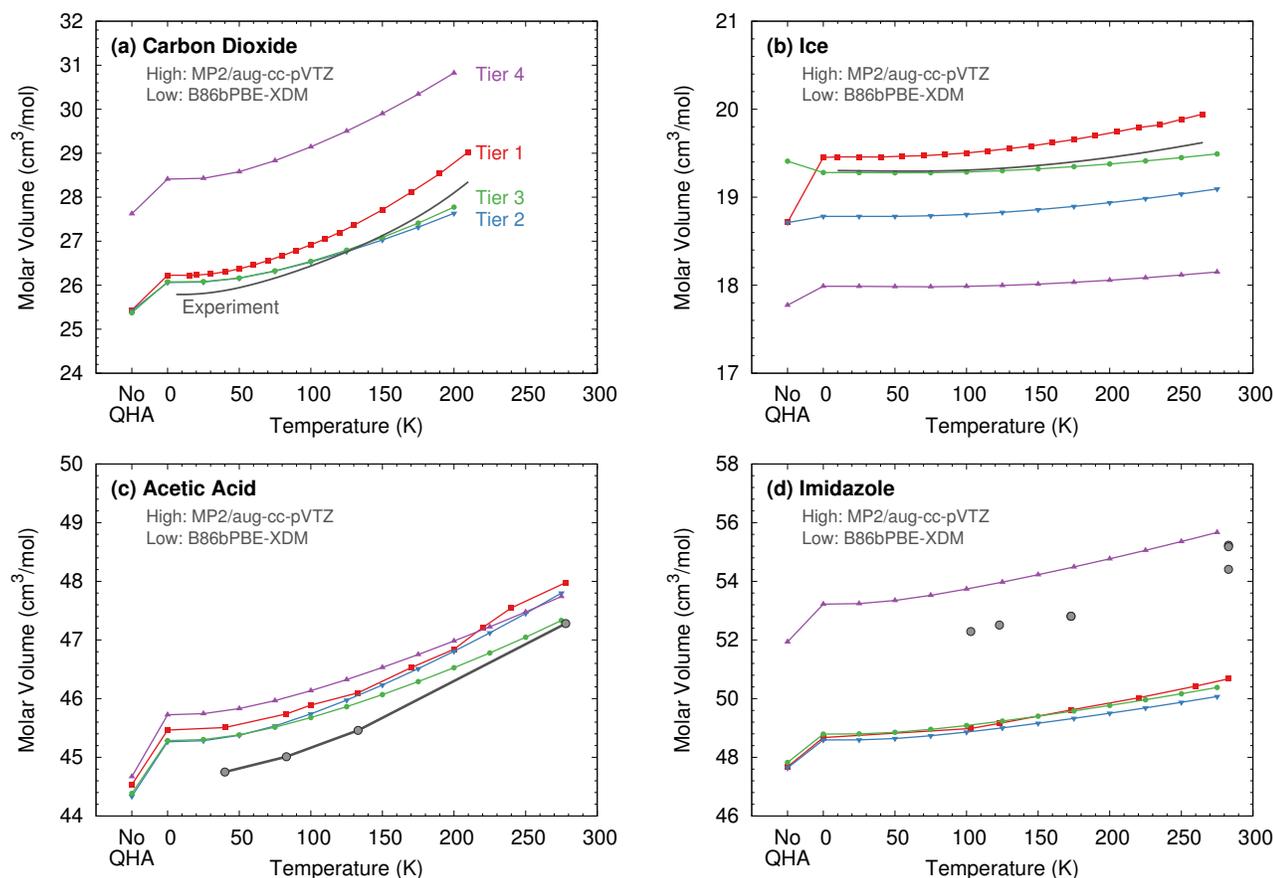
Fig. 2 Comparison of predicted molar volumes from Tiers 1–4 approximations for (a) carbon dioxide, (b) ice, (c) acetic acid, and (d) imidazole using MP2/aug-cc-pVTZ + AMOEBA for the high-level calculations and B86bPBE-XDM for the low level ones. The No QHA data refers to the electronic energy minimum, with no vibrational contribution.

and then combined with MP2 in various basis sets (aug-cc-pVTZ or larger). Extrapolation to the complete basis set limit from the triple and quadruple zeta basis sets was performed in the usual fashion.[80,81] All dimer calculations in HMBI employed a counterpoise correction for basis set superposition error.

Most of the HMBI calculations used the AMOEBA force field for the long-range and many-body contributions. These were evaluated using Tinker 7.1.[82] Existing force field parameters were used for water, acetic acid, and imidazole.[52] Poltype[83] was used to generate parameters for carbon dioxide[43] and acetaminophen. Only the intermolecular force field parameters are needed in the context of HMBI, since intramolecular contributions are treated quantum mechanically.

In select cases, single-point energies were refined with periodic Hartree-Fock and the pob-TZVP basis,[84] which is a variant of def2-TZVP adapted for periodic calculations, and were performed using CRYSTAL09.[85,86] Basis set superposition error is a potential problem in Gaussian basis set calculations on periodic crystals, but addressing it in the context of the many-body calculations here is challenging. This basis was chosen here because an earlier study found that many-body contributions in small molecular clusters computed in the pob-TZVP basis set without counterpoise correction compared well against those from in large basis sets.[46] A 10^{-7} a.u. tolerance was used for the Coulomb overlap

threshold, Coulomb penetration threshold, and exchange overlap threshold, and tolerances of 10^{-12} and 10^{-30} a.u. for the pseudo-overlaps (see Ref 86 for details). Monkhorst-Pack and Gilat shrinking factors of 8 were used for the four smaller crystals, and 4 for acetaminophen.

DFT calculations on carbon dioxide, ice, acetic acid, and imidazole were performed using the periodic boundary planewave/pseudopotential and projector augmented wave (PAW) approaches with an 80 Rydberg energy cutoff and $5\times5\times5$ Monkhorst-Pack k-point grid. For the larger acetaminophen crystal, a lower plane wave energy cutoff of 60 Ry and $1 \times 3 \times 3$ k-point grid were used. DFT energies and gradients were computed with Quantum Espresso v6.1[87,88] and Γ-point frequencies were produced by Phonopy v1.11.2.[89] The BLYP and B86BPBE PAW functionals for H, C, N and O were produced using A. Dal Corso's Atomic code v6.1. Most DFT results reported here were obtained using the B86bPBE functional[90,91] with the Becke-Johnson's exchange-hole dipole method (XDM) dispersion correction,[92] which has performed well in earlier molecular crystal studies.[34,35,92,93] Selected results with other functionals, such as BLYP[94,95] and PBE[91] with the D2[96] or XDM dispersion correction are also presented.

3 Results and Discussion

The work here primarily focuses on phase I carbon dioxide, ice Ih, the orthorhombic phase of acetic acid, and the α form of imidazole. These crystals exhibit diverse non-covalent interactions, ranging from strongly cooperative hydrogen bonding to π systems with significant van der Waals dispersion interactions. Ice and acetic acid are dominated by hydrogen bonded interactions. Ice has the familiar hexagonal pattern and each molecule accepting two and donating two hydrogen bonds (Bernal-Fowler rules), while the acetic acid molecules form one-dimensional chains. Carbon dioxide is bound by a mixture of electrostatics and dispersion, and the π-conjugated imidazole rings form one-dimensional hydrogen-bonded chains with strong dispersion interactions between them.

3.1 Molar volume and thermal expansion

To begin, we examine the performance of Tiers 1–4 on carbon dioxide, ice, acetic acid, and imidazole. We previously examined these crystals with MP2 and various basis sets (Tier 1).[9] With counterpoise corrected dimer energies, smaller basis sets typically underestimate non-covalent attractions. For these crystals modeled with HMBI, this translates to molar volumes being overestimated. In carbon dioxide or ice, for example, systematically increasing the basis set from aug-cc-pVDZ all the way to the complete basis set limit shrinks the molar volume, with the thermal expansion curves in the different basis sets being relatively parallel to one another.[9]

The present study focuses on Tier 1 results at the MP2/aug-cc-pVTZ level for a couple reasons. First, Tier 1 calculations require the energies, geometries, and phonons all be computed at the MP2 level, which is computationally expensive. The aug-cc-pVTZ basis set provides a practical compromise between basis-set completeness and computational efficiency, making Tier 1 calculations feasible on species like acetic acid and imidazole. Second, as shown in Figure 2, this level of theory predicts volumes for carbon dioxide, ice, and acetic acid that are (fortuitously) in reasonably good agreement with experiment. MP2 performs worse for imidazole, since it exaggerates the van der Waals attractions between the molecules, which translates to the underestimated volume seen in Figure 2. The Tier 1 results also generally reproduce the experimentally observed rate of thermal expansion.

Tier 2 replaces the MP2 phonons with ones calculated from DFT (B86bPBE-XDM here). The MP2 phonon frequencies tend to differ moderately from the DFT ones, as shown for ice in Figure 3. Most notably, MP2 predicts excessively large intramolecular frequencies in the O-H stretching region. In inelastic neutron scattering experiments,[97,98] these modes occur in the range $\sim$3000–3500 cm^{-1}, while MP2 predicts them to be several hundred wave numbers higher in energy.[99] DFT calculations provide a much better description of those high-frequency modes. On the other hand, the slightly lower 500–1100 cm^{-1} range of the MP2 librational modes is in better agreement with experiment than the DFT ones, which are shifted about 100 cm^{-1} higher. Both models predict generally similar frequencies for the HOH bending modes near 1600 cm^{-1} and pseudotranslational models below
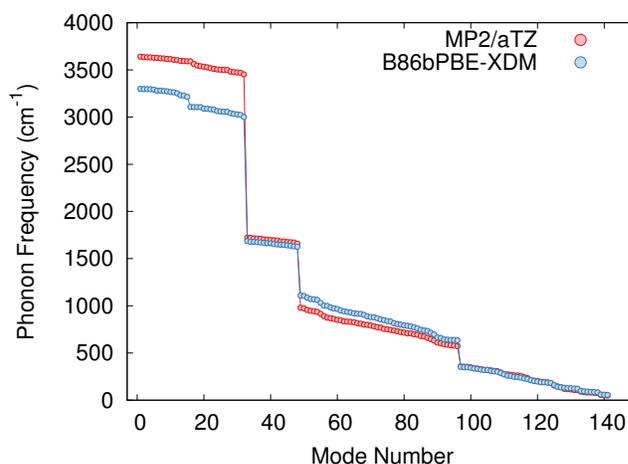
Fig. 3 Comparison of predicted ice phonon frequencies predicted with MP2/aug-cc-pVTZ + AMOEBA or from periodic B86bPBE-XDM.

400 cm^{-1}. See Refs 99 and 100 for more discussion of MP2 and DFT prediction of inelastic neutron scattering spectra in ice. MP2 and DFT phonon frequencies exhibited similar qualitative behaviors relative to experiment in crystalline methanol.[45] Errors in the high-frequency modes will impact the zero-point vibrational energy contribution, but they have a much smaller effect on thermal expansion. Differences in low frequency modes will have a bigger impact on the thermal expansion.

When applied to quasi-harmonic thermal expansion, replacing the MP2 phonon frequencies with DFT ones in Tier 2 introduces only a modest decrease in the quality of the predicted molar volumes. In ice, for example, moving from Tier 1 to Tier 2 with B86bPBE-XDM phonons shrinks the molar volume by a few tenths of a cm^3/mol. Increasing the MP2 basis set further would lead to further volume underestimation.[9] For carbon dioxide, 0 K volumes are similar with Tier 1 and 2, but the thermal expansion is underestimated at Tier 2.

The performance of Tier 3, which uses geometries and phonons computed with B86bPBE-XDM, is generally very similar to Tier 2. The largest molar volume differences occur for ice, where the two models differ by up to $\sim$1 cm^3/mol. For acetic acid, they agree very closely at low temperature, but differ by $\sim$0.5 cm^3/mol near room temperature. The differences between Tiers 2 and 3 are even smaller in the other two crystals.

However, Tier 3 ice exhibits the unusual feature that adding the zero-point vibrational energy contribution (i.e. from "No QHA" to 0 K in Figure 2b) actually leads to a 0.1 cm^3/mol lattice contraction, instead of the typical expansion. This does not occur for Tier 4, which uses the same phonons. As shown in ESI Figure S2, the quasi-harmonic B86bPBE-XDM vibrational free energy exhibits a shallow minimum at 18 cm^3/mol. For Tier 4 B86bPBE-XDM, the electronic energy minimum occurs at smaller volume, where F_{vib} has negative slope, so adding the zero-point contribution leads to expansion. On the other hand, the Tier 3 MP2 electronic energy minimum occurs above 19 cm^3/mol, in the regime where the B86bPBE-XDM vibrational free energy has a positive slope, and adding zero-point vibrational energy drives an initial contraction.
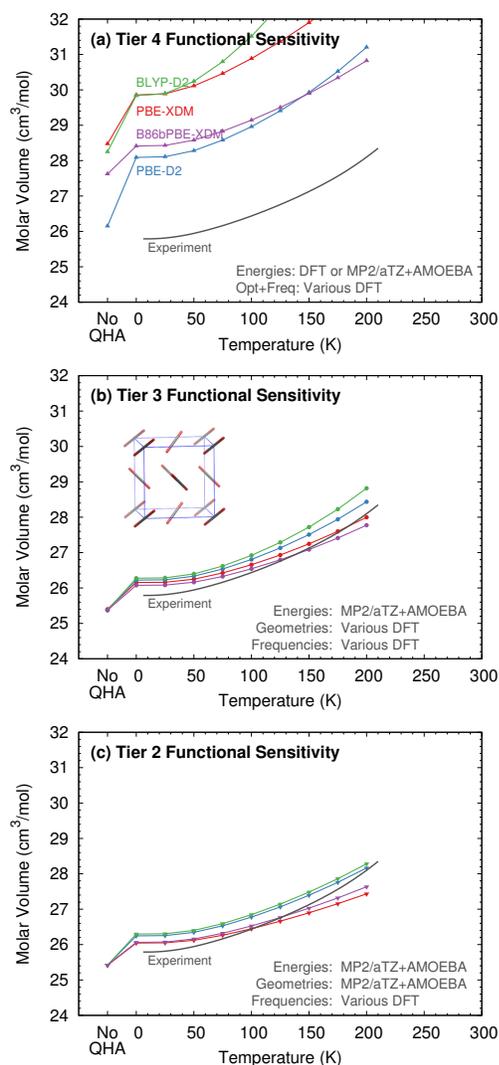
Fig. 4 (a) While different density functionals predict somewhat different molar volumes for carbon dioxide (Tier 4), the sensitivity of the predicted volumes decreases considerably when (b) MP2 single-points are used on the DFT geometries (Tier 3), and (c) it decreases further when only the DFT phonons are used (Tier 2).

At higher temperatures, the F_{vib} minima shift toward larger volumes, allowing expansion to occur in Tier 3. Interestingly, this minimum in F_{vib} does not occur for MP2 phonons (Tier 1). In Tier 2, the minimum occurs at larger volumes and does not cause the contraction seen in Tier 3. In other words, this behavior appears to be an unfortunate artifact of the Tier 3 combination of MP2 energies with DFT geometries and phonons. Nevertheless, the actual predicted molar volumes are reasonable.

Finally, employing pure B86bPBE-XDM (Tier 4) also predicts the molar volumes rather accurately. It significantly overestimates the molar volume in carbon dioxide, but it performs well for the other three crystals. Notably, B86bPBE-XDM reproduces the experimental molar volume in imidazole fairly well, where MP2 significantly overbinds the crystal and underestimates the volume due to its well-known problems describing van der Waals dispersion.[101] That MP2 problem will be addressed below.

Interestingly, the Tier 2 and 3 (and to a lesser extent Tier 4) results here tend to exhibit less thermal expansion than Tier 1. One possible explanation could be that the former included only Γ-point phonons, while the Tier 1 results from Ref 9 include lattice dynamical phonon dispersion. We previously showed that including phonon dispersion increased the predicted rate of thermal expansion.[43] Supercell phonon calculations quickly become computationally demanding in DFT. With the fragment HMBI approach, on the other hand, they can be performed with very little additional cost over the Γ-point only calculation, since the unique additional contributions in the supercell are handled at the MM level. Other more subtle factors involving the interplay between the $E(V)$ curves and F_{vib} contributions likely contribute as well. In acetic acid, for instance, the Tier 2 model expands more rapidly with temperature than Tier 3, despite both neglecting phonon dispersion.

Ice Ih is unusual in that it exhibits negative thermal expansion, with the volume contracting by around 0.06% between 10 K and 70 K, before expanding. Most of the models studied here reproduce this trend qualitatively, though fewer are quantitatively correct. We previously found that Tier 1 MP2/CBS + AMOEBA predicts a slight contraction of only 0.1% and at at a lower 40 K. Interestingly, a different MP2-based fragment study[102] also predicted the contraction in the aug-cc-pVDZ and aug-cc-pVTZ basis sets, though they found that MP2 exaggerated the contraction and predicted the minimum at higher temperatures. The discrepancy between those results and our earlier ones might result from the use of counterpoise correction in our work, which leads to underbinding of the crystal, versus no counterpoise correction in Ref 102, which will lead to overbinding. Counterpoise correction will impact the balance between the key hydrogen bonding phonon modes and hydrogen stretching modes.

Here, we examine how the hybrid approaches behave. ESI Figure S5 plots the relative molar volumes at low temperature for several representative methods from Tiers 2, 3, and 4. While Tier 2 MP2/aug-cc-pVTZ + AMOEBA demonstrates negligible contraction of the lattice, the Tier 3 and Tier 4 results perform somewhat better. They correctly predict the location of the minimum near 60–70 K, but they underestimate the amount of contraction at only 0.02–0.03%.

Taken together, these results reiterate that dispersion-corrected density functionals like B86bPBE-XDM can predict thermal expansion well. Tier 1 MP2 molar volumes and thermal expansion often differ from the DFT ones, but refining the single-point energies with MP2 already corrects for much of that difference. Such single-point energy refinements can be achieved with relatively modest additional computational cost. The further advantages of Tier 2 or Tier 1 for molar volumes are somewhat smaller, and will not be computationally worthwhile for predicting structural parameters in many applications.

Of course, these results represent only the B86bPBE-XDM functional. Additional insight is obtained by considering the behavior of Tiers 2–4 with several different density functionals and either the XDM or D2 dispersion correction. Figure 4a plots the predicted thermal expansion with four different functionals: BLYP-D2, PBE-D2, PBE-XDM, and B86bPBE-XDM. The functionals
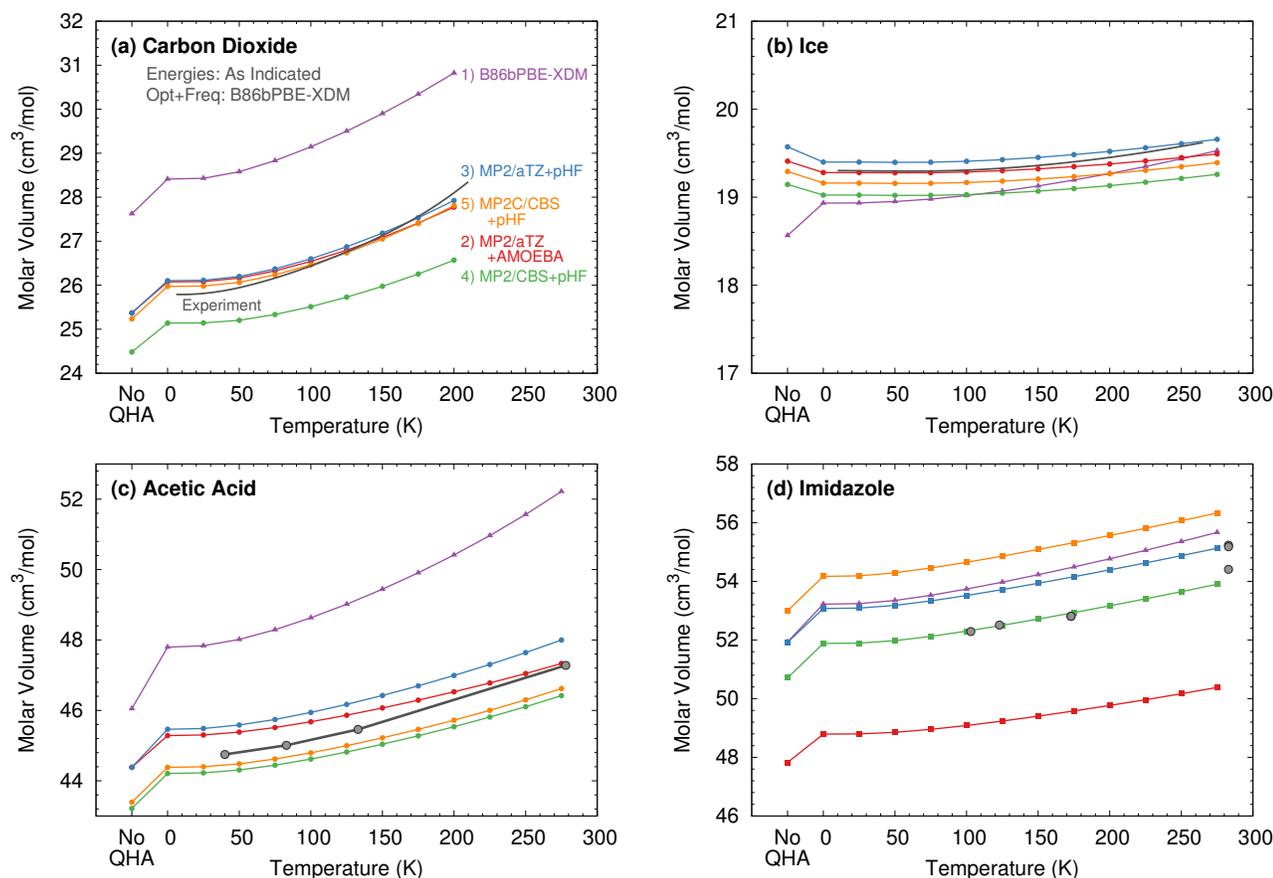
Fig. 5 Impact of single-point HMBI energy refinement on the DFT predictions for (a) carbon dioxide, (b) ice, (c) acetic acid, and (d) imidazole. Starting with (1) pure B86bPBE (Tier 4), we (2) first refine to Tier 3 with MP2/aug-cc-pVTZ + AMOEBA. Further Tier 3 refinements are made by (3) replacing the AMOEBA many-body treatment with a periodic HF one, (4) extrapolating MP2 to the complete basis set limit, and (5) correcting MP2 with MP2C.

overestimate the 0 K molar volume by ∼10–15%, and the rate of thermal expansion differs considerably between the D2 and XDM dispersion corrections. Models corrected with D2 generally predict larger thermal expansion than those employing XDM. Because they derive their dispersion coefficients directly from electronic structure dispersion models like XDM, Tkatchenko-Scheffler (TS),[103] or many-body dispersion (MBD),[104–106] are generally expected to be superior to a purely empirical correction like D2.[107] The D3 or D4 models,[108,109] which adapts the dispersion coefficients based on the chemical environment would provide a better comparison, but those are not currently implemented in Quantum Espresso.

Regardless, focus not on the performance of specific density functionals and/or dispersion corrections, but rather what happens when ingredients from those functionals are used in Tier 2 or 3 calculations. As shown in Figures 4b, simply refining the calculations with MP2 single point energies (Tier 3) dramatically reduces the sensitivity of the calculations to the density functional used to optimize the structures and compute the phonons. At Tier 2, where only the phonons are obtained from DFT, the sensitivity of the predicted molar volumes to the functional decreases further. Additional sensitivity data is provided in ESI Figures S6 and S7. These results suggest that although the DFT geometries defining the $E(V)$ curve clearly differ from each

other and the MP2/aug-cc-pVTZ ones, single-point energy refinement renormalizes much of the variations among them and gives $E(V)$ curves in generally good agreement with one another. In this context, it is also worth noting that density functional tight binding proved successful in modeling the thermal expansion in carbamazepine, and this could provide another route to low-cost phonons for Tiers 2 and 3.[37]

Given the good performance and relatively low computational cost of using HMBI-refined single-point energies with DFT optimizations and phonons (Tier 3), the next question is to see how reliably one can predict the molar volumes by further improving the quality of the HMBI single-point energies. These energies can be refined in three ways. First, one might increase the basis set size from aug-cc-pVTZ to the complete basis set limit via a triple-zeta/quadruple-zeta extrapolation. The counterpoise-corrected energies tend to underestimate the interactions in small basis sets, leading to overestimation of the molar volume.[9]

Second, one could replace the AMOEBA many-body treatment with one from periodic HF. Recent work found that AMOEBA overestimates many-body polarization associated with the cooperative hydrogen bonding in crystalline methanol, and refining the energetics with periodic HF proved important for obtaining the correct phase diagram.[46] Similar over-polarization is found for AMOEBA treatments of ion-water interactions.[110] Strong po-

larization effects are present in several of the crystals here, so there could be appreciable benefits to periodic HF refinement here as well.

Third, MP2 exhibits well-known problems with the treatment of van der Waals dispersion.[101] Among the four crystals here, this is most apparent for imidazole, where MP2 substantially overbinds the lattice energy[38,39] and underestimates the molar volume (see Figure 2d).[9] Ideally, one would correct this problem by replacing MP2 with CCSD(T). However, dispersion-corrected MP2C[76,77] provides a more pragmatic approach which corrects most of the MP2 error in these crystals at much lower computational cost.[79]

Figure 5 examines this hierarchy of refinements for the four crystals. As seen in the earlier discussion of Figure 2, switching from (1) pure B86bPBE-XDM (Tier 4) to (2) Tier 3 MP2/aug-cc-pVTZ + AMOEBA single-point energies leads to a substantial change in the predicted molar volumes, usually toward smaller unit cells (the slight volume increase in ice is the exception). (3) Replacing the AMOEBA many-body contribution with periodic HF increases the molar volume. For carbon dioxide, ice, and acetic acid, the effect is fairly small. For imidazole, on the other hand, it increases the volume by $\sim$9%. As expected, (4) increasing the MP2 basis set toward the CBS limit induces a volume contraction of $\sim$0.4 cm^3/mol in ice and around 1 cm^3/mol in the other three crystals. With the exception of imidazole, the MP2/CBS + periodic HF predicted volumes are slightly smaller than experiment. Surprisingly, in imidazole, the MP2/CBS + periodic HF volumes agree very well with experiment, despite MP2's overestimation of the lattice energy. In all four cases, (5) MP2C weakens the binding and shifts toward larger molar volumes. Unsurprisingly, the largest corrections are observed for carbon dioxide and imidazole, while hydrogen bonded ice and acetic acid are less affected by the dispersion correction.

Overall, the combination of MP2C/CBS + periodic HF energies on B86bPBE-XDM geometries and phonons predicts the highest-temperature experimental molar volumes of carbon dioxide, ice, and acetic acid to within 1–2%. For imidazole, the errors are 2% or 3.5%, depending on which high-temperature experimental structure one compares against. Finally, notice that the different possible Tier 3 single-point energy refinements considered here all predict similar thermal expansivity (curves (2)–(5) in Figure 5 are largely parallel). The most significant variations manifest as shifts in the 0 K molar volume. This reflects that while the minimum of the $E(V)$ curves shifts upon single-point energy refinement, changes to the potential energy well curvature are apparently minor (see ESI Figure S8).

3.2 Thermochemical data

A key reason for modeling thermal expansion in molecular crystals is to predict temperature-dependence of other crystal properties. Accordingly, we consider the enthalpy and entropy of sublimation for these four crystals. Experimental values were taken and/or derived from the literature as described in Refs 9 and 43. Quantitative experimental uncertainties are not readily available for the thermochemical properties presented here.

The temperature-dependent results were frequently derived using data from a variety of sources that did not always report uncertainties. Moreover, different studies do not always agree (e.g. reported room-temperature sublimation enthalpies for imidazole differ by several kJ/mol[111]). Crystalline defects in the experimental solids can also play a role. Forming a point defect is typically an endothermic process, but it also leads to a gain in entropy. Quantifying the impact of the various factors here is difficult, but one should probably allow for uncertainties of up to a few kJ/mol in the sublimation enthalpies, for example.

Figure 6 compares sublimation enthalpies as predicted with several of the techniques described in the previous section against experiment. Given the relatively small improvements in molar volume provided by Tier 2 over Tier 3, the discussion here focuses primarily on Tiers 3 and 4. Unless otherwise mentioned, all DFT results in this section employ B86bPBE-XDM.

As temperature increases, the sublimation enthalpy $\Delta H_{sub} = H_{gas} - H_{crystal}$ typically first increases before reaching a maximum and then decreasing. Heating increases H_{gas} via destabilizing translational, rotational, and PV contributions. $H_{crystal}$ derives from a balance between the thermal expansion and the vibrational contributions, but it is typically dominated by lattice energy destabilization due to thermal expansion. Little thermal expansion occurs in the crystal at low temperatures, and the ΔH_{sub} increases due primarily to the gas contribution in that temperature regime. At higher temperatures, however, the larger thermal expansion in the crystal eventually leads to the increase in $H_{crystal}$ becoming more significant than the changes in H_{gas}, which produces the maximum and subsequent decrease in ΔH_{sub} seen for carbon dioxide, acetic acid, and imidazole. In ice, this maximum does not occur below the melting point due to the low thermal expansivity. See Ref 9 for more detailed discussion of the enthalpy behaviors.

Earlier Tier 1 work[9,43] demonstrated that changing the electronic structure method and basis set shifts the entire sublimation curves vertically but has minor impact on the curvature. Larger basis sets in particular shift the enthalpy toward larger values. Obtaining the proper maximum and subsequent decrease of the sublimation enthalpy at higher temperatures requires capturing thermal expansion correctly. A simple harmonic model that neglects thermal expansion agrees well with the quasi-harmonic result at low temperatures, but it overestimates the enthalpy at higher temperatures by about 1 kJ/mol in these crystals. Ice proves the exception: since it exhibits comparatively little thermal expansion, the error introduced in ΔH_{sub} by neglecting that expansion at 273 K is negligible.

In the present work, the Tier 2-3 results frequently underestimate the amount of thermal expansion compared to Tier 1. In Figure 6, this underestimated thermal expansion manifests in the Tier 3 MP2/aug-cc-pVTZ + AMOEBA sublimation enthalpy (red curve) being too large at higher temperatures, analogously to what was observed for the harmonic model.[9] Nevertheless, those Tier 3 results generally mimic the Tier 1 ones to within 1–2 kJ/mol across the full temperature range.

Refining Tier 1 by increasing the basis set size to the CBS limit, applying the MP2C dispersion correction, and replacing AMOEBA
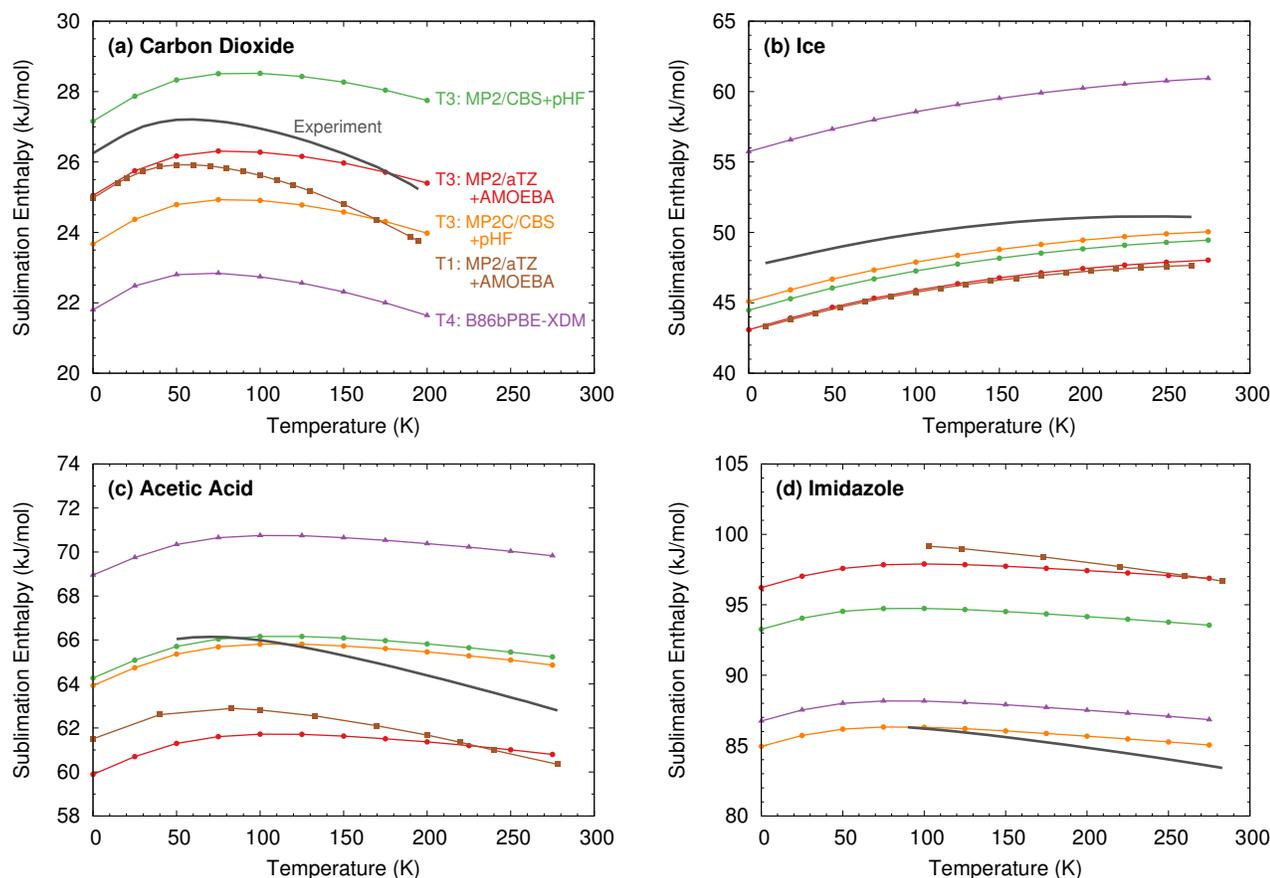
Fig. 6 Comparison of predicted sublimation enthalpies for (a) carbon dioxide, (b) ice, (c) acetic acid, and (d) imidazole using Tier 1 (T1) MP2/aug-cc-pVTZ + AMOEBA, Tier 4 (T4) B86bPBE-XDM, and Tier 3 (T3) with several different energy refinements.

with periodic HF does not resolve the issue of the erroneous slope in ΔH_{sub} at higher temperatures. Nevertheless, MP2C/CBS + periodic HF results (orange curve) provide excellent agreement with experiment across the temperature range, with root-mean-square (rms) errors ranging 0.9–2.1 kJ/mol for the four crystals (Table 2). Applying the dispersion correction in MP2C has minimal impact on hydrogen-bonded ice and acetic acid, but it alters the sublimation enthalpies in carbon dioxide and imidazole considerably (compare green vs. orange curves). In our earlier work, Tier 1 MP2/CBS and CCSD(T)/CBS both overestimated the sublimation enthalpy for carbon dioxide, with CCSD(T) predicting a slightly smaller ΔH_{sub}.[9,43] Here, it appears that MP2C overcorrects the MP2 result, with the net result of slightly increasing the rms error from 1.7 to 2.1 kJ/mol. On the other hand, MP2C performs very well for imidazole, reducing the rms error in ΔH_{sub} from 9.2 kJ/mol (MP2) to 0.8 kJ/mol (MP2C).

Compared to the best Tier 3 MP2C results, the errors for B86bPBE-XDM are 2–3 times larger for carbon dioxide and imidazole, where van der Waals dispersion contributes appreciably, and 5–6 times larger for acetic acid and ice, which are dominated by hydrogen bonding interactions (Table 2). Notably, B86bPBE-XDM performs very well for imidazole, which is problematic for MP2. Overall, the sublimation enthalpy data here bolsters the case for Tier 3 single-point energy refinement with MP2C/CBS + periodic HF on top of the DFT structures and phonons.

Next, consider prediction of the sublimation entropy. Whereas $H_{crystal}$ is dominated by the lattice energy and therefore sensitive to the final single-point energy, $S_{crystal}$ is governed by the phonon frequencies. Tiers 2–4 all compute the phonons with DFT. The improved energies in Tier 2 or Tier 3 will alter the predicted volume at a given temperature, which in turn impacts the phonons via their volume dependence (Eq 5).

Like for the enthalpy, the temperature dependence of the sublimation entropy $\Delta S_{sub}(T) = S_{gas}(T) - S_{crystal}(T)$ arises from a competition between the entropy of the gas phase and the crystal phase.[9] At low temperatures, $S_{gas}(T)$ rises more quickly with temperature. At higher temperatures, the situation reverses, with $S_{crystal}(T)$ increasing more quickly due to the phonon contribution. Together, these produce the overall concave shape of $\Delta S_{sub}(T)$. If thermal expansion is not accounted for, the phonon frequencies tend to be too large, and $S_{crystal}(T)$ will be too small. This causes overestimation of the entropy at high temperatures.

Here, the thermal expansion is frequently underestimated relative both to experiment and Tier 1 calculations. This translates to consistent overestimation of $\Delta S_{sub}(T)$ by up to 10–12% relative to experiment at high temperatures (Figure 7). In cases like ice and acetic acid, where the volume is not too sensitive to specific method used for Tier 3 energy refinement, the variation in predicted sublimation entropies is fairly small across the different energy models. Larger variations are observed among the different

Table 2 Root-mean-square error (in kJ/mol) between predicted and experimental sublimation enthalpies over the temperatures for which experimental data is available (see in Figure 6). Errors were computed by splining the data curves and taking differences between them at 1 K intervals.

Crystal	Temperature Range	Tier 3 MP2/CBS+pHF	Tier 3 MP2C/CBS+pHF	Tier 4 B86bPBE-XDM
Carbon Dioxide	0–195 K	1.7	2.1	4.2
Ice	10–265 K	2.5	1.9	8.9
Acetic Acid	50–278 K	1.3	1.0	5.6
Imidazole	90–283 K	9.2	0.9	2.6

Tier 3 models for imidazole and and carbon dioxide, commensurate with the greater sensitivity of the molar volumes to the modeling approach in those crystals. Overall, in marked contrast to the molar volumes and sublimation enthalpies, Tier 3 energy refinement does not clearly improve the quality the underlying DFT entropies. The same can be said for Tier 2 (not shown), since the Tier 2 and 3 sublimation entropies differ by less than 1%.

Calculating phase transition temperatures provides another means of assessing predicted thermochemistry values, since the transition temperature can be sensitive to subtle changes in the Gibbs free energy.[9,43,46] Computing the Gibbs free energy accurately requires balance between the enthalpic and entropic components, which may or many not be maintained in the hybrid approaches.

Experimentally, carbon dioxide sublimes at 194.7 K and atmospheric pressure.[64] Table 3 summarizes predicted sublimation temperatures with several different methods. Large-basis Tier 1 MP2 and CCSD(T) perform excellently, predicting the sublimation temperature of 5 degrees Kelvin of experiment. In smaller basis sets, it underestimates the sublimation temperature. At the other extreme, B86bPBE-XDM underestimates the sublimation temperature by almost 40 K. Tier 3 refinement at the MP2 level improves the predicted sublimation temperature somewhat, though the Tier 3 temperatures are ∼10 K lower than the corresponding Tier 1 ones. As noted earlier, MP2C seemingly over-corrects MP2, to the detriment of the predicted sublimation temperature. The ∼30 K error in the MP2C/CBS + periodic HF sublimation temperature is only modestly better than that of B86bPBE-XDM.

Table 3 Comparison of experimental and predicted sublimation temperatures for carbon dioxide.

Tier	Method	T_{sub} (K)
	Experiment[a]	194.7
Tier 1	MP2/aDZ + AMOEBA[b]	163.6
Tier 1	MP2/aTZ + AMOEBA[b]	185.3
Tier 1	MP2/aQZ + AMOEBA[b]	193.4
Tier 1	MP2/CBS + AMOEBA[b]	199.2
Tier 1	CCSD(T)/CBS + AMOEBA[b]	201.0
Tier 3	MP2/aTZ + AMOEBA	174.2
Tier 3	MP2/CBS + pHF	186.6
Tier 3	MP2C/CBS + pHF	165.7
Tier 4	B86bPBE-XDM	157.5

[a] Ref 64   [b] Ref 43
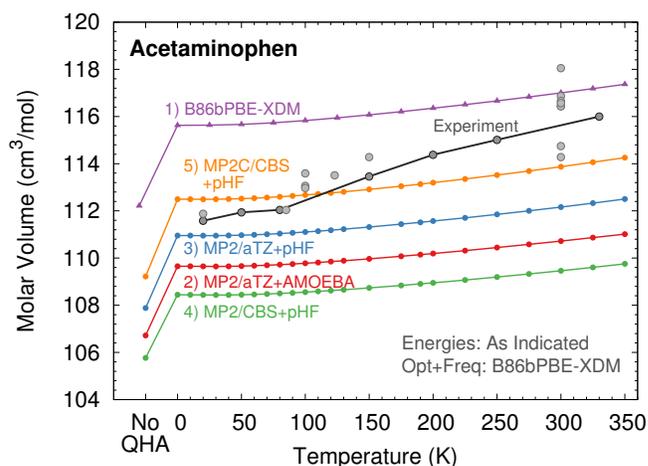
Fig. 8 Predicted acetaminophen molar volumes versus temperature. The connected dark gray points indicate data from a temperature-dependent neutron scattering study,[57] while light gray points represent other experimental data points found in the CSD.

3.3 Acetaminophen form I

To investigate how well these models perform in a pharmaceutically relevant species, Figure 8 plots thermal expansion data for acetaminophen. Twenty two experimental crystal structures of ambient pressure form I have been reported in the CSD. While most of the reported molar volumes exhibit reasonable agreement, a wide ∼4 cm^3/mol scatter exists in the reported room temperature values. Seven of the structures (those connected with a line in Figure 8) come from a single temperature-dependent neutron scattering study.[57] The discussion below focuses primarily on this consistent set of neutron scattering data.

Given the large size of acetaminophen ($C_8H_9NO_2$ and $Z = 4$ in form I), calculations were only performed at Tiers 3 and 4. Tiers 1 and 2 would require substantially more computational effort. With a predicted molar volume of 115.6 cm^3/mol at 20 K, Tier 4 B86bPBE-XDM overestimates the experimental molar volume of 111.6 cm^3/mol (HXACAN13[57]) by 3.6%. It also significantly underestimates the thermal expansivity, with the B86bPBE-XDM molar volume increasing only 1.3% versus 3.8% experimentally. The combination of overestimated volume at low temperature and underestimated thermal expansivity leads to much smaller errors in the molar volumes at high temperatures, e.g. only 1% error at 330 K (HXACAN19[57]).

Switching to Tier 3 with MP2/aug-cc-pVTZ + AMOEBA leads to a considerable reduction in the molar volume to 109.65 cm^3/mol, which is in somewhat better agreement with experiment (1.7%
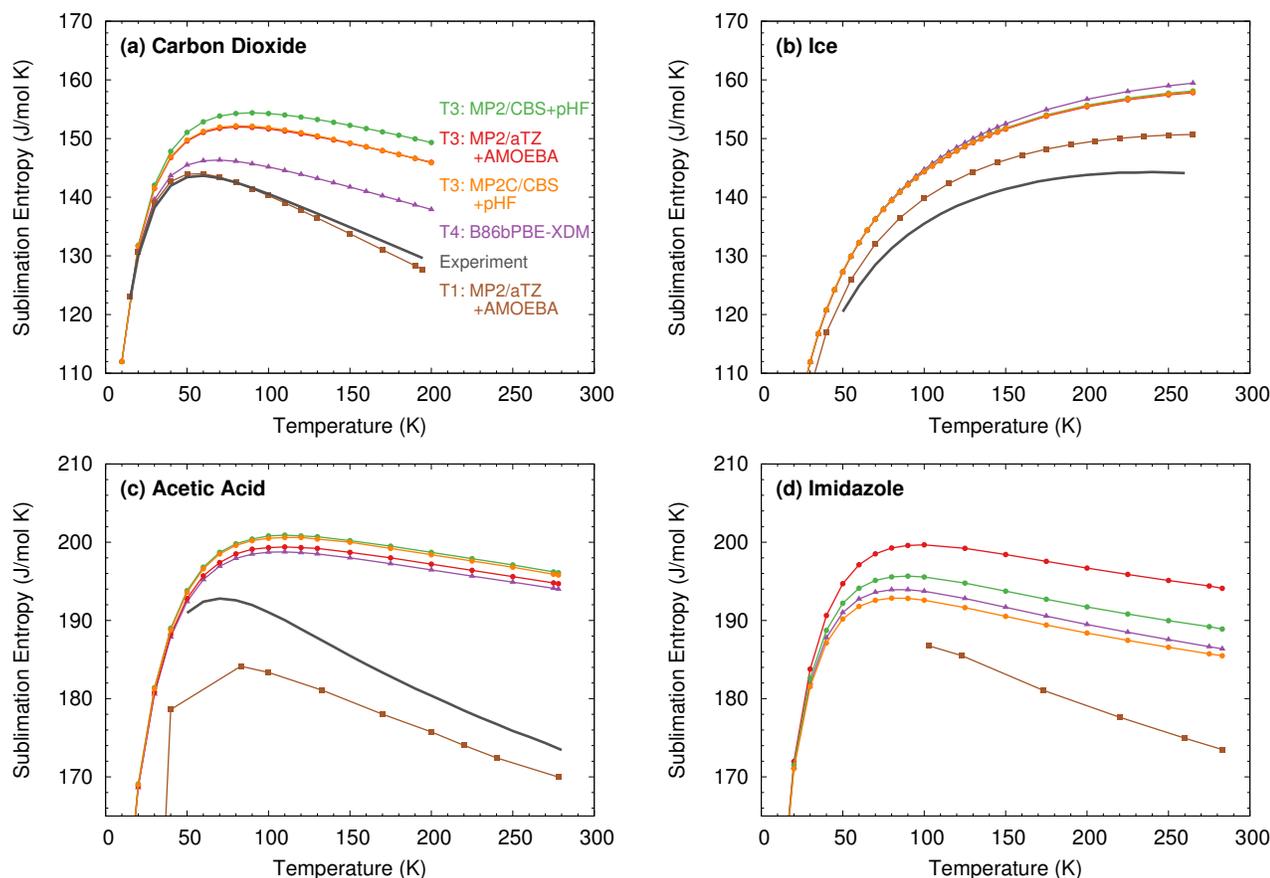
Fig. 7 Comparison of predicted sublimation entropies for (a) carbon dioxide, (b) ice, (c) acetic acid, and (d) imidazole using Tier 1 MP2/aug-cc-pVTZ + AMOEBA, Tier 4 B86bPBE-XDM, and Tier 3 with several different energy refinements. Experimental entropy data is unavailable for imidazole.

error at 20 K). However, the underestimated thermal expansivity persists, and the volume at 330 K is underestimated by 4.4%. Moving toward the CBS limit, replacing MP2 with MP2C and AMOEBA with periodic HF both shift back toward larger molar volumes, but they have little impact on the thermal expansivity. In the end, the MP2C/CBS + periodic HF volumes are fairly close to experiment, especially at low temperatures (0.8% error at 20 K), but they underestimate the volume by 1.6% at 330 K due to the low thermal expansivity.

Next, we turn to the form I acetaminophen sublimation enthalpy and entropy. Perlovich and co-workers measured $\Delta H_{sub}(298K) = 117.9\pm0.7$ kJ/mol from vapor pressure measurements,[112,113] while Picciochi at al subsequently obtained 129.9 ± 1.4 kJ/mol from a combination of vapor pressure measurements and microcalorimetry experiments (and they proposed a slight refinement of Perlovich's value to 118.9 ± 1.6 kJ/mol).[114] The ~10 kJ/mol discrepancy between the experimental values is significantly larger than the reported 1–2 kJ/mol experimental uncertainties. The quasi-harmonic calculations here can address this discrepancy.

Table 4 compares the predicted and experimental room-temperature sublimation enthalpies. Tier 4 B86bPBE-XDM predicts 131.0 kJ/mol, which lies within the stated uncertainty in Picciochi et al's value of 129.9 ± 1.4 kJ/mol. MP2 predicts a sublimation enthalpy that is up to 23 kJ/mol higher, but employing

MP2C/CBS + periodic HF reduces this enthalpy to 138.0 kJ/mol. This is 8 kJ/mol larger than the Picciochi et al experimental value. Some of this overestimation may stem from the underpredicted thermal expansion, as seen for acetic acid and imidazole earlier. In any case, both the MP2C and B86bPBE-XDM results support the larger 129.9 ± 1.4 experimental sublimation enthalpy instead of the smaller 117.9 ± 0.7 kJ/mol value.

Finally, Perlovich et al reported a sublimation entropy of 190 ± 2 J/(mol K) at 298 K. Tier 4 B86bPBE-XDM and various Tier 3 refinements all predict much larger values of 240–246 J/(mol K). Overestimation of the sublimation entropy is expected based on the results for the other crystals described above and by how much the predictions underestimate the thermal expansion. Still, this ~25% disagreement between theory and experiment is significantly larger than the ~10–12% seen in the smaller crystals. On the other hand, it is not clear how reliable the reported experimental entropy value is, since it was derived from the sublimation enthalpy measurement[112] which is suspect in light of the Picciochi et al experiments[114] and our calculations here.

4 Conclusions

The combination of fragment-based correlated wavefunction electronic structure techniques and quasi-harmonic approximations can be very successful in predicting thermal expansion and other properties, at least for rigid-molecule crystals. On the other hand,

Table 4 Comparison of experimental and predicted 298 K sublimation enthalpies (kJ/mol) and entropies (J/(mol K)) for acetaminophen form I.

Method	Source	ΔH_{sub} (298 K)	ΔS_{sub} (298 K)
Perlovich et al	Ref 112,113	117.9 ±0.7	190 ± 2
Picciochi et al	Ref 114	129.9 ± 1.4	
B86bPBE-XDM	Tier 4	131.0	242.1
MP2/aTZ+AMOEBA	Tier 3	146.4	245.6
MP2/aTZ+pHF	Tier 3	147.4	244.8
MP2/CBS+pHF	Tier 3	154.1	246.3
MP2C/CBS+pHF	Tier 3	138.0	243.9

dispersion-corrected DFT models also often perform well at appreciably lower computational cost. By comparing a hierarchy of models ranging from pure DFT to pure MP2, we have demonstrated that introducing correlated wavefunction energies on top of DFT geometries and phonons can appreciably improve predicted molar volumes and enthalpies. One must ensure, however, that the single-point energies are well-chosen, which in practice means employing large basis sets and accounting for any deficiencies in the models (e.g. by replacing MP2 with MP2C for the monomer and dimer contributions or AMOEBA with HF for the many-body contributions).

In the small molecule crystals, the hybrid Tier 3 approach led to predicting molar volumes to within a few percent and sublimation enthalpies to within 1–2 kJ/mol of experiment over broad temperature ranges. Though more computationally expensive than pure DFT approaches, such single-point energy refinement can be performed on crystals containing dozens of atoms per molecule, especially when crystal symmetry can be exploited. Using these techniques, we demonstrated that the predicted sublimation enthalpy for acetaminophen agrees better with the more recent experimental value of Picciochi et al than the earlier reported value.

Issues remain, however. The hybrid approaches that combine DFT and wavefunction techniques do not appreciably improve the predicted entropies, since those are largely governed by phonon contributions. We also found that the hybrid calculations here generally underestimate the amount of thermal expansion. In the smaller crystals the impact was modest, but it becomes more significant in acetaminophen. Acetaminophen also exhibited considerably larger 8 kJ/mol errors in the predicted sublimation enthalpy than for the smaller crystals. Accounting for phonon dispersion might help, but anharmonicity or other factors may also play an important role. More testing in larger, more flexible molecules is needed to assess the performance of the quasi-harmonic approach. Efficient and effective strategies for addressing anharmonicity would be especially valuable.

Moreover, though the performance of the hybrid approaches is quite good, it may not always be sufficient. The imbalances between the enthalpy and entropy appreciably increased the error in the predicted carbon dioxide sublimation temperature, for example. More dramatically, in our recent study of the methanol phase diagram,[46] even a half kJ/mol error in the relative free energies between two polymorphs shifts the phase transition temperature by ∼100 K. For such challenging properties, more reliable and computationally demanding Tier 1 approaches may be needed.

Conflicts of interest

There are no conflicts to declare.

Notes and references

1 S. L. Price, *Chem. Soc. Rev.*, 2014, **43**, 2098–111.
2 S. L. Price, D. E. Braun and S. M. Reutzel-Edens, *Chem. Commun.*, 2016, **52**, 7065–7077.
3 S. L. Price and S. M. Reutzel-Edens, *Drug Disc. Today*, 2016, **21**, 912–923.
4 G. M. Day, T. G. Cooper, A. J. Cruz-Cabeza, K. E. Hejczyk, H. L. Ammon, S. X. M. Boerrigter, J. S. Tan, R. G. Della Valle, E. Venuti, J. Jose, S. R. Gadre, G. R. Desiraju, T. S. Thakur, B. P. van Eijck, J. C. Facelli, V. E. Bazterra, M. B. Ferraro, D. W. M. Hofmann, M. A. Neumann, F. J. J. Leusen, J. Kendrick, S. L. Price, A. J. Misquitta, P. G. Karamertzanis, G. W. A. Welch, H. A. Scheraga, Y. A. Arnautova, M. U. Schmidt, J. van de Streek, A. K. Wolf and B. Schweizer, *Acta Cryst. B*, 2009, **65**, 107–125.
5 D. A. Bardwell, C. S. Adjiman, Y. A. Arnautova, E. Bartashevich, S. X. M. Boerrigter, D. E. Braun, A. J. Cruz-Cabeza, G. M. Day, R. G. Della Valle, G. R. Desiraju, B. P. van Eijck, J. C. Facelli, M. B. Ferraro, D. Grillo, M. Habgood, D. W. M. Hofmann, F. Hofmann, K. V. J. Jose, P. G. Karamertzanis, A. V. Kazantsev, J. Kendrick, L. N. Kuleshova, F. J. J. Leusen, A. V. Maleev, A. J. Misquitta, S. Mohamed, R. J. Needs, M. A. Neumann, D. Nikylov, A. M. Orendt, R. Pal, C. C. Pantelides, C. J. Pickard, L. S. Price, S. L. Price, H. A. Scheraga, J. van de Streek, T. S. Thakur, S. Tiwari, E. Venuti and I. K. Zhitkov, *Acta Cryst. B*, 2011, **67**, 535–551.
6 A. M. Reilly, R. I. Cooper, C. S. Adjiman, S. Bhattacharya, A. D. Boese, J. G. Brandenburg, P. J. Bygrave, R. Bylsma, J. E. Campbell, R. Car, D. H. Case, R. Chadha, J. C. Cole, K. Cosburn, H. M. Cuppen, F. Curtis, G. M. Day, R. A. DiStasio Jr, A. Dzyabchenko, B. P. van Eijck, D. M. Elking, J. A. van den Ende, J. C. Facelli, M. B. Ferraro, L. Fusti-

Molnar, C.-A. Gatsiou, T. S. Gee, R. de Gelder, L. M. Ghiringhelli, H. Goto, S. Grimme, R. Guo, D. W. M. Hofmann, J. Hoja, R. K. Hylton, L. Iuzzolino, W. Jankiewicz, D. T. de Jong, J. Kendrick, N. J. J. de Klerk, H.-Y. Ko, L. N. Kuleshova, X. Li, S. Lohani, F. J. J. Leusen, A. M. Lund, J. Lv, Y. Ma, N. Marom, A. E. Masunov, P. McCabe, D. P. McMahon, H. Meekes, M. P. Metz, A. J. Misquitta, S. Mohamed, B. Monserrat, R. J. Needs, M. A. Neumann, J. Nyman, S. Obata, H. Oberhofer, A. R. Oganov, A. M. Orendt, G. I. Pagola, C. C. Pantelides, C. J. Pickard, R. Podeszwa, L. S. Price, S. L. Price, A. Pulido, M. G. Read, K. Reuter, E. Schneider, C. Schober, G. P. Shields, P. Singh, I. J. Sugden, K. Szalewicz, C. R. Taylor, A. Tkatchenko, M. E. Tuckerman, F. Vacarro, M. Vasileiadis, A. Vazquez-Mayagoitia, L. Vogt, Y. Wang, R. E. Watson, G. A. de Wijs, J. Yang, Q. Zhu and C. R. Groom, *Acta Cryst. B*, 2016, **72**, 439–459.

7   S. L. Price, *Int. Rev. Phys. Chem.*, 2008, **27**, 541–568.

8   J. Nyman and G. M. Day, *Phys. Chem. Chem. Phys.*, 2016, **18**, 31132–31143.

9   Y. N. Heit and G. J. O. Beran, *Acta Cryst. B*, 2016, **72**, 514–529.

10 A. Gavezzotti and G. Filippini, *J. Am. Chem. Soc.*, 1995, **117**, 12299–12305.

11 J. Hoja, A. M. Reilly and A. Tkatchenko, *WIREs Comput. Mol. Sci.*, 2017, **7**, e1294.

12 P. Raiteri, R. Martoňák and M. Parrinello, *Angew. Chem. Int. Ed.*, 2005, **44**, 3769–73.

13 P. G. Karamertzanis, P. Raiteri, M. Parrinello, M. Leslie and S. L. Price, *J. Phys. Chem. B*, 2008, **112**, 4298–308.

14 T. Zykova-Timan, P. Raiteri and M. Parrinello, *J. Phys. Chem. B*, 2008, **112**, 13231–7.

15 A. M. Reilly, S. Habershon, C. A. Morrison and D. W. H. Rankin, *J. Chem. Phys.*, 2010, **132**, 134511.

16 T.-Q. Yu and M. Tuckerman, *Phys. Rev. Lett.*, 2011, **107**, 015701.

17 E. Schneider, L. Vogt and M. E. Tuckerman, *Acta Cryst. B*, 2016, **72**, 542–550.

18 M. J. Schnieders, J. Baltrusaitis, Y. Shi, G. Chattree, L. Zheng, W. Yang and P. Ren, *J. Chem. Theory Comput.*, 2012, **8**, 1721–1736.

19 I. J. Nessler, J. M. Litman and M. J. Schnieders, *Phys. Chem. Chem. Phys.*, 2016, 36–38.

20 E. C. Dybeck, N. P. Schieber and M. R. Shirts, *J. Chem. Theory Comput.*, 2016, acs.jctc.6b00397.

21 E. C. Dybeck, N. S. Abraham, N. P. Schieber and M. R. Shirts, *Crystal Growth and Design*, 2017, **17**, 1775–1787.

22 J. Nyman and G. M. Day, *CrystEngComm*, 2015, **17**, 5154–5165.

23 S. A. Rivera, D. G. Allis and B. S. Hudson, *Cryst. Growth Des.*, 2008, **8**, 3905–3907.

24 N. Marom, R. A. DiStasio, V. Atalla, S. Levchenko, A. M. Reilly, J. R. Chelikowsky, L. Leiserowitz and A. Tkatchenko, *Angew. Chem. Int. Ed.*, 2013, **52**, 6629–6632.

25 S. Wen and G. J. O. Beran, *J. Chem. Theory Comput.*, 2012,

8, 2698–2705.

26 A. M. Reilly and A. Tkatchenko, *Phys. Rev. Lett.*, 2014, **113**, 055701.

27 D. E. Braun, J. A. McMahon, L. H. Koztecki, S. L. Price and S. M. Reutzel-Edens, *Cryst. Growth Des.*, 2014, **14**, 2056–2072.

28 G. Filippini, C. M. Gramaccioli, M. Simonetta and G. B. Suffritti, *Chem. Phys. Lett.*, 1975, **35**, 17–20.

29 G. Filippini and C. M. Gramaccioli, *Acta Cryst. A*, 1981, **37**, 335–342.

30 B. P. van Eijck, *J. Comp. Chem.*, 2001, **22**, 816–826.

31 G. M. Day and S. L. Price, *J. Am. Chem. Soc.*, 2003, **125**, 16434–43.

32 G. M. Day, S. L. Price and M. Leslie, *J. Phys. Chem. B*, 2003, **107**, 10919–10933.

33 E. Sanz, C. Vega, J. Abascal and L. MacDowell, *Phys. Rev. Lett.*, 2004, **92**, 255701.

34 S. R. Whittleton, A. Otero-de-la Roza and E. R. Johnson, *J. Chem. Theory Comput.*, 2017, **13**, 441–450.

35 S. R. Whittleton, A. Otero-de-la Roza and E. R. Johnson, *J. Chem. Theory Comput.*, 2017, **13**, 5332–5342.

36 A. Erba, J. Maul and B. Civalleri, *Chem. Commun.*, 2016, **52**, 1820–1823.

37 J. G. Brandenburg, J. Potticary, H. A. Sparkes, S. L. Price and S. R. Hall, *J. Phys. Chem. Lett.*, 2017, **8**, 4319–4324.

38 G. J. O. Beran and K. Nanda, *J. Phys. Chem. Lett.*, 2010, **1**, 3480–3487.

39 S. Wen and G. J. O. Beran, *J. Chem. Theory Comput.*, 2011, **7**, 3733–3742.

40 K. Nanda and G. J. O. Beran, *J. Chem. Phys.*, 2012, **137**, 174106.

41 Y. Heit and G. J. O. Beran, *J. Comp. Chem.*, 2014, **35**, 2205–2214.

42 G. J. O. Beran, J. D. Hartman and Y. N. Heit, *Acc. Chem. Res.*, 2016, **49**, 2501–2508.

43 Y. N. Heit, K. D. Nanda and G. J. O. Beran, *Chem. Sci.*, 2016, **7**, 246–255.

44 W. Sontising, Y. N. Heit, J. L. McKinley and G. J. O. Beran, *Chem. Sci.*, 2017, **8**, 7374–7382.

45 C. Červinka and G. J. O. Beran, *Phys. Chem. Chem. Phys.*, 2017, **19**, 29940–29953.

46 C. Červinka and G. J. O. Beran, , 2018, **submitted**,.

47 C. Červinka, M. Fulem, R. P. Stoffel and R. Dronskowski, *Journal of Physical Chemistry A*, 2016, **120**, 2022–2034.

48 C. Červinka and M. Fulem, *J. Chem. Theory Comput.*, 2017, **13**, 2840–2850.

49 H. Stoll, *Chem. Phys. Lett.*, 1992, **191**, 548–552.

50 C. Müller and B. Paulus, *Phys. Chem. Chem. Phys.*, 2012, **14**, 7605–7614.

51 G. J. O. Beran, *Chem. Rev.*, 2016, **116**, 5567–5613.

52 P. Ren, C. Wu and J. W. Ponder, *J. Chem. Theory Comput.*, 2011, **7**, 3143–3161.

53 W. H. Keesom and J. W. L. Kohler, *Physica*, 1934, **1**, 655–658.

54 I. Morrison, J.-C. Li, S. Jenkins, S. S. Xantheas and M. C. Payne, *J. Phys. Chem. B*, 1997, **101**, 6146–6150.

55 I. Nahringbauer, *Acta Chem. Scand.*, 1970, **24**, 453.

56 R. K. McMullan, J. Epstein, J. R. Ruble and B. M. Craven, *Acta Cryst. B*, 1979, **35**, 688–691.

57 R. Boese, B. D, R. Latz and A. Bäumen, *Z. Kristallogr.*, 2000, **215**, 693–701.

58 I. N. Krupskii, A. Prokhvatilov, A. I. Erenburg and A. S. Barylnik, *Fiz. Nizk. Temp.*, 1982, **8**, 533.

59 V. F. Petrenko and R. W. Whitworth, *Physics of Ice*, Oxford University Press, 1999.

60 P. Jönson, *Acta Cryst.*, 1971, **B27**, 893–898.

61 B. M. Craven, R. K. McMullan, J. D. Bell and H. C. Freeman, *Acta Cryst. B*, 1977, **B33**, 2585.

62 G. Will, *Z.Kristallogr.,Kristallgeom.,Kristallphys.,Kristallchem.*, 1969, **129**, 211.

63 M. Azreg-Aïnou, *Monatshefte fur Chemie*, 2005, **136**, 2017–2027.

64 W. F. Giauque and C. J. Egan, *J. Chem. Phys.*, 1937, **5**, 45.

65 G. Herzberg, *Electronic Spectra and Electronic Structure of Polyatomic Molecules*, D. Van Nostrand Company, Inc, 1966.

66 T. Shimanouchi, *Tables of Molecular Vibrational Frequencies*, United States Department of Commerce, 1972, vol. 1.

67 R. Feistel and W. Wagner, *Geochim. Cosmochim. Acta*, 2007, **71**, 36–45.

68 NIST/TRC Web Thermo Tables (WTT), NIST Standard Reference Subscription Database 2—Lite Edition Version 2-2012-1-Lite.

69 *Handbook of Chemistry and Physics*, ed. W. M. Haynes, CRC Press, 96th edn., 2004.

70 S. Verevkin, *J. Chem. Eng. Data*, 2000, **45**, 953.

71 J. Martin and R. L. Andon, *J. Chem. Thermo.*, 1982, **14**, 679.

72 P. Jiménez and C. T. M.V. Roux, *J. Chem. Thermo.*, 1987, **19**, 985.

73 H. G. M. De Wit, C. G. De Kruif and J. C. Van Miltenburg, *J. Chem. Thermo.*, 1983, **15**, 891.

74 F. Billes, H. Endrédi and G. Jalsovszky, *J. Mol. Struct. (Theochem)*, 1999, **465**, 157.

75 MOLPRO, version 2012.1, a package of ab initio programs, H.-J. Werner, P. J. Knowles, G. Knizia, F. R. Manby, M. Schütz, P. Celani, T. Korona, R. Lindh, A. Mitrushenkov, G. Rauhut, K. R. Shamasundar, T. B. Adler, R. D. Amos, A. Bernhardsson, A. Berning, D. L. Cooper, M. J. O. Deegan, A. J. Dobbyn, F. Eckert, E. Goll, C. Hampel, A. Hesselmann, G. Hetzer, T. Hrenar, G. Jansen, C. Köppl, Y. Liu, A. W. Lloyd, R. A. Mata, A. J. May, S. J. McNicholas, W. Meyer, M. E. Mura, A. Nicklass, D. P. O'Neill, P. Palmieri, D. Peng, K. Pflüger, R. Pitzer, M. Reiher, T. Shiozaki, H. Stoll, A. J. Stone, R. Tarroni, T. Thorsteinsson, and M. Wang, see http://www.molpro.net.

76 A. Hesselmann, *J. Chem. Phys.*, 2008, **128**, 144112.

77 M. Pitonak and A. Hesselmann, *J. Chem. Theory Comput.*, 2010, **6**, 168–178.

78 L. A. Burns, M. S. Marshall and C. D. Sherrill, *J. Chem. Phys.*, 2014, **141**, 234111.

79 Y. Huang, Y. Shao and G. J. O. Beran, *J. Chem. Phys.*, 2013, **138**, 224112.

80 A. Karton and J. M. L. Martin, *Theor. Chem. Acc.*, 2006, **115**, 330–333.

81 T. Helgaker, W. Klopper, H. Koch and J. Noga, *J. Chem. Phys.*, 1997, **106**, 9639–9646.

82 J. W. Ponder, TINKER v7.1, 2015, http://dasher.wustl.edu/tinker/, Accessed September 21, 2016.

83 J. C. Wu, G. Chattree and P. Ren, *Theor. Chem. Acc.*, 2012, **131**, 1138.

84 M. F. Peintinger, D. V. Oliveira and T. Bredow, *J. Comp. Chem.*, 2013, **34**, 451–459.

85 R. Dovesi, R. Orlando, B. Civalleri, C. Roetti, V. R. Saunders and C. M. Zicovich-Wilson, *Z. Kristallogr.*, 2005, **220**, 571–573.

86 R. Dovesi, V. R. Saunders, C. Roetti, R. Orlando, C. M. Zicovich-Wilson, F. Pascale, B. Civalleri, K. Doll, N. M. Harrison, I. J. Bush, P. D'Arco, M. Llunell, C. Science and A. Technologies, *CRYSTAL09 User's Manual*, University of Torino, Torino, 2009.

87 P. Giannozzi, S. Baroni, N. Bonini, M. Calandra, R. Car, C. Cavazzoni, D. Ceresoli, G. L. Chiarotti, M. Cococcioni, I. Dabo, A. Dal Corso, S. de Gironcoli, S. Fabris, G. Fratesi, R. Gebauer, U. Gerstmann, C. Gougoussis, A. Kokalj, M. Lazzeri, L. Martin-Samos, N. Marzari, F. Mauri, R. Mazzarello, S. Paolini, A. Pasquarello, L. Paulatto, C. Sbraccia, S. Scandolo, G. Sclauzero, A. P. Seitsonen, A. Smogunov, P. Umari and R. M. Wentzcovitch, *J. Phys. Condens. Mat.*, 2009, **21**, 395502.

88 P. Giannozzi, O. Andreussi, T. Brumme, O. Bunau, M. Buongiorno Nardelli, M. Calandra, R. Car, C. Cavazzoni, D. Ceresoli, M. Cococcioni, N. Colonna, I. Carnimeo, A. Dal Corso, S. de Gironcoli, P. Delugas, R. A. DiStasio, A. Ferretti, A. Floris, G. Fratesi, G. Fugallo, R. Gebauer, U. Gerstmann, F. Giustino, T. Gorni, J. Jia, M. Kawamura, H.-Y. Ko, A. Kokalj, E. Küçükbenli, M. Lazzeri, M. Marsili, N. Marzari, F. Mauri, N. L. Nguyen, H.-V. Nguyen, A. Otero-de-la Roza, L. Paulatto, S. Poncé, D. Rocca, R. Sabatini, B. Santra, M. Schlipf, A. P. Seitsonen, A. Smogunov, I. Timrov, T. Thonhauser, P. Umari, N. Vast, X. Wu and S. Baroni, *J. Phys. Condens. Mat.*, 2017, **29**, 465901.

89 A. Togo and I. Tanaka, *Scr. Mater.*, 2015, **108**, 1–5.

90 A. D. Becke, *J. Chem. Phys.*, 1986, **38**, 7184–7187.

91 J. P. Perdew, K. Burke and M. Ernzerhof, *Phys. Rev. Lett.*, 1996, **77**, 3865.

92 A. Otero-de-la Roza and E. R. Johnson, *J. Chem. Phys.*, 2012, **136**, 174109.

93 A. Otero-De-La-Roza, B. H. Cao, I. K. Price, J. E. Hein and E. R. Johnson, *Angew. Chem. Int. Ed.*, 2014, **53**, 7879–7882.

94 A. D. Becke, *Phys. Rev. A*, 1988, **38**, 3098–3100.

95 C. Lee, W. Yang and R. G. Parr, *Phys. Rev. B*, 1988, **37**, 785–789.

96 S. Grimme, *J. Comp. Chem.*, 2006, **16**, 1787–1799.

97 J. Li and D. K. Ross, *Nature*, 1993, **365**, 327–329.

98 J. Li, *J. Chem. Phys.*, 1996, **105**, 6733–6755.

99 X. He, O. Sode, S. S. Xantheas and S. Hirata, *J. Chem. Phys.*, 2012, **137**, 204505.

100 P. Zhang, L. Tian, Z. P. Zhang, G. Shao and J. C. Li, *J. Chem. Phys.*, 2012, **137**, 044504.

101 K. E. Riley, M. Pitonak, P. Jurecka and P. Hobza, *Chem. Rev.*, 2010, **110**, 5023–63.

102 M. A. Salim, S. Y. Willow and S. Hirata, *J. Chem. Phys.*, 2016, **144**, 204503.

103 A. Tkatchenko and M. Scheffler, *Phys. Rev. Lett.*, 2009, **102**, 073005.

104 R. A. DiStasio, O. A. von Lilienfeld and A. Tkatchenko, *Proc. Nat. Acad. Sci.*, 2012, **109**, 14791–14795.

105 A. Tkatchenko, R. A. DiStasio, R. Car and M. Scheffler, *Phys. Rev. Lett.*, 2012, **108**, 236402.

106 A. Ambrosetti, A. M. Reilly, R. A. DiStasio and A. Tkatchenko, *J. Chem. Phys.*, 2014, **140**, 18A508.

107 S. Grimme, A. Hansen, J. G. Brandenburg and C. Bannwarth, *Chem. Rev.*, 2016, **116**, 5105–5154.

108 S. Grimme, J. Antony, S. Ehrlich and H. Krieg, *J. Chem. Phys.*, 2010, **132**, 154104.

109 E. Caldeweyher, C. Bannwarth and S. Grimme, *J. Chem. Phys.*, 2017, **147**, 034112.

110 O. Demerdash, Y. Mao, T. Liu, M. Head-Gordon and T. Head-Gordon, *The Journal of Chemical Physics*, 2017, **147**, 161721.

111 W. Acree and J. S. Chickos, *J. Phys. Chem. Ref. Data*, 2010, **39**, 043101.

112 G. L. Perlovich, T. V. Volkova and A. Bauer-Brandl, *J. Therm. Anal. Cal.*, 2007, **89**, 767–774.

113 G. L. Perlovich, T. V. Volkova and A. BauerâĂŘBrandl, *Journal of Pharmaceutical Sciences*, 2006, **95**, 2158–2169.

114 R. Picciochi, H. P. Diogo and M. E. Minas da Piedade, *J. Therm. Anal. Cal.*, 2010, **100**, 391–401.
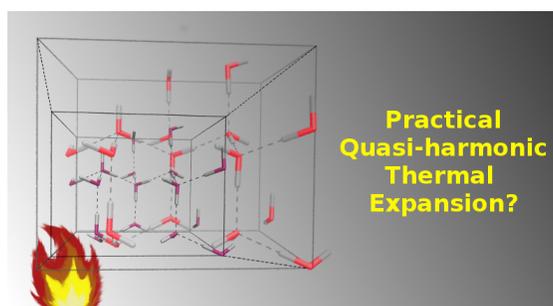
Fig. 9 Table of Contents Entry: Hybrid quasi-harmonic electronic structure strategies predict molecular crystal thermal expansion and thermochemistry in good agreement with experiment with reasonable computational cost.